Z. Phys. B 103, 391–400 (1997)

ZEITSCHRIFT
FÜR PHYSIK B

Quantum molecular dynamics study of the Su-Schrieffer-Heeger model

Kristel Michielsen, Hans De Raedt

Institute for Theoretical Physics and Materials Science Centre, University of Groningen, Nijenborgh 4, 9747 AG Groningen, The Netherlands

Received: 22 November 1996

Abstract. A quantum molecular dynamics technique is presented to compute the static and dynamic properties of a system of fermions coupled to classical degrees of freedom. The method is employed to investigate the properties of the Su-Schrieffer-Heeger model, an electron-phonon model which is often used to describe the electronic properties of conjugated polymers. The Su-Schrieffer-Heeger model is shown to exhibit a metal-insulator transition away from half-filling. In the metallic phase the electron transport is collective and shows the features characteristic of Fröhlich conductivity. Our simulation data for the optical absorption at room-temperature are in good agreement with experiment.

PACS: 71.10.+x; 71.38.+i; 74.20.-z

1. Introduction

There is a vast class of physical systems that may, as a first step, be modelled in terms of quantum mechanical degrees of freedom interacting with a set of classical variables. Models of this kind are used to describe for example, solvated electrons [1], metallic clusters [2], the electronic properties of polymers [3–5], f- and d-electron systems [6], crystallization [7, 8], etc. Usually the classical environment itself displays complicated dynamical behavior and one often has to resort to a Molecular Dynamics or Monte Carlo simulation to unravel its properties. Methods have been developed to compute the time-independent properties of the quantum mechanical system embedded in the classical environment [1,9,10].

In this paper we will focus on models described by the Hamiltonian

$$H = \sum_{i,j}\sum_{s} c^{+}_{i,s} T^{(s)}_{i,j}(\{u_k\},\mu) c_{j,s} + \frac{1}{2M}\sum_i p_i^2 + \frac{1}{2}\sum_{i,j} u_i K_{i,j} u_j, \quad (1)$$

Dedicated to Prof. Wolfgang Götze on the occasion of his 60th birthday

where $c^{+}_{i,s}$ and $c_{i,s}$ are the creation and annihilation operators, respectively, for an electron with spin $s =\uparrow,\downarrow$ at the generalized site index i, u_i is the phonon coordinate, p_i is the corresponding momentum and M denotes the mass of the oscillators. $T^{(s)}_{i,j}(\{u_k\},\mu)$ specifies the free-electron energy for a fixed lattice deformation (e.g. the hopping matrix elements (if $i \neq j$) as well as the local potential (if $i = j$)), and is assumed to be a linear function of the phonon coordinates $\{u_k\}$. As we will work in the grand canonical ensemble throughout, it is convenient to absorb in $T^{(s)}_{i,j}$ the term proportional to the chemical potential μ. $K_{i,j}$ is the matrix of oscillator spring constants. Both $T^{(s)}_{i,j}$ and $K_{i,j}$ are Hermitian matrices. The number of lattice sites will be denoted by L.

Hamiltonian (1) describes the interaction of electrons and lattice deformations, and is sufficiently general to encompass all standard electron-phonon models such as the Holstein model, the Su-Schrieffer-Heeger (SSH) model, etc.. The purpose of this work is to demonstrate that for models of type (1) one can compute the *dynamical* properties of the quantum degrees of freedom directly with roughly the same accuracy as the time-independent quantities. A key point thereby is the absence, in (1), of terms representing electron-electron interactions.

2. Static properties

A straightforward application of standard Quantum Monte Carlo (QMC) methods [11], although feasible in principle, is fraught with difficulties in particular for the applications we will discuss below (see Sect. 4). This is due to the fact that (i) for the temperature range of interest the standard QMC methods suffer from severe numerical instabilities and (ii) it is extremely difficult to compute the dynamic properties at these temperatures. Therefore we take a different route which is tailored to the situation at hand and is based on the following rigorous results.

To study the statistical mechanical properties of the model, an expression is needed for the grand-canonical partition function $Z \equiv \mathbf{tr}\exp(-\beta H) = \int_{\{u_k\}} \rho(\{u_k\})$, β denoting the inverse temperature. An upperbound to the partition function can be found by decomposing Hamiltonian (1) as $H = H_1 + H_2$, where

$$H_1 = \frac{1}{2M}\sum_i p_i^2$$
$$H_2 = \sum_{i,j}\sum_s c_{i,s}^+ T_{i,j}^{(s)}(\{u_k\},\mu)c_{j,s} + \frac{1}{2}\sum_{i,j} u_i K_{i,j} u_j \ . \qquad (2)$$

Application of inequality [12–14]

$$Z \le \widetilde{Z} \equiv \mathbf{Tr} e^{-\beta H_1} e^{-\beta H_2} = \mathbf{Tr} e^{-\beta H_1/2} e^{-\beta H_2} e^{-\beta H_1/2} \ , \qquad (3)$$

yields for the partition function

$$Z \le \left(\frac{M}{2\pi\beta\hbar^2}\right)^{L/2} \int_{\{u_k\}} e^{-\beta\sum_{i,j} u_i K_{i,j} u_j/2} \times \mathbf{tr}\exp\left(-\beta\sum_{i,j}\sum_s c_{i,s}^+ T_{i,j}^{(s)}(\{u_k\},\mu)c_{j,s}\right) \ . \qquad (4)$$

Expression (4) directly follows from the path-integral representation of Z if one neglects the imaginary-time dependence of the phonon coordinates. Since H is a quadratic form in the fermionic degrees of freedom, the trace **tr** over the fermions can be performed analytically, yielding for the partition function

$$Z \le \left(\frac{M}{2\pi\beta\hbar^2}\right)^{L/2} \int_{\{u_k\}} e^{-\beta\sum_{i,j} u_i K_{i,j} u_j/2} \times \prod_s \det\left(1 + e^{-\beta T^{(s)}(\{u_k\},\mu)}\right) \ . \qquad (5)$$

A lower bound to the partition function can be found using the linearity of the electron-phonon interaction. Writing Hamiltonian (1) as $H = H_3 + H_4$ with

$$H_3 = \frac{1}{2M}\sum_i p_i^2 + \sum_{i,j}\frac{(u_i-\overline{u}_i)K_{i,j}(u_j-\overline{u}_j)}{2} + \sum_{i,j}\frac{\overline{u}_i K_{i,j}\overline{u}_j}{2} + \sum_{i,j}\sum_s c_{i,s}^+ T_{i,j}^{(s)}(\{\overline{u}_k\},\mu)c_{j,s}$$
$$H_4 = \sum_{i,j}\frac{(u_i-\overline{u}_i)K_{i,j}\overline{u}_j + \overline{u}_i K_{i,j}(u_j-\overline{u}_j)}{2} + \sum_{i,j}\sum_s c_{i,s}^+ T_{i,j}^{(s)}(\{u_k-\overline{u}_k\},\mu)c_{j,s} \ , \qquad (6)$$

application of a generalized form of Jensen 's inequality [15]

$$\mathbf{Tr} e^{-\beta H_3} e^{\beta H_3} e^{-\beta H} \ge \exp\left(\frac{\mathbf{Tr} e^{-\beta H_3}(-\beta H_4)}{\mathbf{Tr} e^{-\beta H_3}}\right) \times \mathbf{Tr} e^{-\beta H_3}, \qquad (7)$$

yields for the partition function

$$Z \ge Z_p \max_{\overline{u}_k} e^{-\beta\sum_{i,j}\overline{u}_i K_{i,j}\overline{u}_j/2} \times \prod_s \det\left(1 + e^{-\beta T^{(s)}(\{\overline{u}_k\},\mu)}\right) \ , \qquad (8)$$

where

$$Z_p \equiv \mathbf{tr} e^{-\beta H_p} \ , \qquad (9a)$$
$$H_p = \frac{1}{2M}\sum_i p_i^2 + \frac{1}{2}\sum_{i,j} u_i K_{i,j} u_j \ , \qquad (9b)$$

are the partition function and Hamiltonian of the free phonon system respectively.
Combining (5) and (8), the upper and lower bounds to the ground-state energy read

$$\widetilde{E}_0 \le E_0 \le E_0^{(p)} + \widetilde{E}_0 \ , \qquad (10)$$

where $E_0^{(p)}$ is the ground-state energy of the phonon system and

$$\widetilde{E}_0 = \min_{\{u_k\}}\left[\sum_{i,j}\frac{u_i K_{i,j} u_j}{2} - \lim_{\beta\to\infty}\sum_s \mathbf{Sp}\ln\left(1 + e^{-\beta T^{(s)}(\{u_k\},\mu)}\right)\right] \ , \qquad (11)$$

where $\mathbf{Sp}X$ denotes the trace of the $L \times L$ matrix X.

In general for models of type (1), the approximation

$$e^{-\beta H} \approx e^{-\beta H_1/2} e^{-\beta H_2} e^{-\beta H_1/2} \ , \qquad (12)$$

is expected to be accurate if β is small (high temperature) or the mass M of the oscillators is large. Approximation (12) is tantamount to a semi-classical treatment of the phonon coordinates [16]. From (10) it follows that if $E_0^{(p)} \ll |\widetilde{E}_0|$, treating the phonon degrees of freedom as classical variables will be a good approximation. At zero temperature, taking this limit is equivalent to making the adiabatic approximation in which the phonon coordinates are determined by minimizing the expectation value of H_2.

Expressions for any static property of interest can be derived in a manner similar to the one used to obtain (5). Expectation values of static quantities are calculated as follows: For a particular configuration $\{u_k\}$ we diagonalize the $L \times L$ matrix T, compute the product of determinants in (5), and multiply the latter by the exponential prefactor, to obtain the weight of the configuration $\{u_k\}$. This weight is strictly positive and can be used directly in a Metropolis Monte Carlo simulation of the variables $\{u_k\}$ to calculate the averages of time-independent quantities. Our algorithm samples the full phase space and is, by construction, free of minus-sign problems or numerical instabilities [11]. The latter enables us to cover a much wider range of temperatures than the one which is usually accessible to other QMC methods [17].

3. Dynamic properties

For models of type (1), the time-dependent quantities can be calculated directly, in the *real-time* domain, without invoking procedures [17] to extrapolate imaginary-time data to the real-time axis.

3.1. Single-particle density of states

The single-particle density of states (DOS) $N(\omega)$ is the probability for removing or adding a single electron from or to the system and is defined as

$$N(\omega) = \frac{1}{2\pi L}\sum_{l,s}\int_{-\infty}^{+\infty} d\tau e^{i\omega\tau}\langle\{c_{l,s}(\tau), c_{l,s}^{+}\}\rangle \ . \tag{13}$$

Using the fact that (1) is a quadratic form of the fermion operators, the time evolution of the annihilation operator in (13) can be worked out analytically, yielding in the semi-classical limit

$$L^{-1}\sum_{l,s}\langle\{c_{l,s}(\tau), c_{l,s}^{+}\}\rangle = Z^{-1}\sum_{s}\int_{\{u_k\}}\rho(\{u_k\}) \times \mathbf{Sp}e^{-i\tau T^{(s)}(\{u_k\},\mu)} \ . \tag{14}$$

Since, in the simulation, we already know the eigenvalues and eigenvectors of $T^{(s)}(\{u_k\},\mu)$, it is straightforward to compute the real and imaginary part of $e^{-i\tau T^{(s)}(\{u_k\},\mu)}$ for arbitrary τ. For each choice of τ, the calculation of $\mathbf{Sp}e^{-i\tau T^{(s)}(\{u_k\},\mu)}$ takes of the order of L operations per configuration $\{u_k\}$, the statistical errors being comparable to those of the static quantities. In practice we choose a set of τ-values (typically 512) such that, after all samples have been taken, the integral in (14) can be computed by Fast Fourier Transformation.

3.2. Optical conductivity and Drude weight

When a pulse of electric field is applied in a particular direction the linear response in this direction is given by $\sigma(\tau) = -i\langle[P(-\tau), J]\rangle$, where $J = i[H, P] = i\sum_{k\neq l}\sum_{s} T_{k,l}^{(s)}(\{u_k\},\mu)\left(c_{k,s}^{+}c_{l,s} - c_{l,s}^{+}c_{k,s}\right)$ is the current operator and $P = \sum_l l n_l$ is the polarization operator. The time evolution of the polarization operator is defined as $P(\tau) = e^{i\tau H}Pe^{-i\tau H}$. In the semi-classical limit $\sigma(\tau) = -i\langle[e^{-i\tau H_2}Pe^{i\tau H_2}, J]\rangle = -i\langle[P, e^{i\tau H_2}Je^{-i\tau H_2}]\rangle$.
The Kubo formula for the optical conductivity reads [18]

$$\sigma(\omega) = \lim_{\epsilon\to 0}\frac{1}{\omega + i\epsilon}\left\{-i\sum_{l,s}\langle\left[lc_{l,s}^{+}c_{l,s}, J\right]\rangle + i\int_0^{\infty} e^{i\omega\tau}e^{-\epsilon\tau}\langle[J, J(\tau)]\rangle d\tau\right\} . \tag{15}$$

The time evolution of the current operator $J(\tau) = e^{i\tau H_2}Je^{-i\tau H_2}$ can be worked out analytically, yielding

$$J(\tau) = i\sum_{i\neq j}\sum_{k,l}\sum_{s} T_{i,j}^{(s)}(\{u_k\},0) \times\left[\left(e^{i\tau T^{(s)}(\{u_k\},\mu)}\right)_{k,i}\left(e^{-i\tau T^{(s)}(\{u_k\},\mu)}\right)_{j,l}c_{k,s}^{+}c_{l,s} - \left(e^{i\tau T^{(s)}(\{u_k\},\mu)}\right)_{l,j}\left(e^{-i\tau T^{(s)}(\{u_k\},\mu)}\right)_{i,k}c_{l,s}^{+}c_{k,s}\right] . \tag{16}$$

The analytical expression for the expectation value of the commutator appearing in (15) reads

$$\langle[J, J(\tau)]\rangle = -2iZ^{-1}\int_{\{u_k\}}\sum_{i,j}\sum_{s}\rho(\{u_k\})\left(1 + e^{\beta\lambda_i}\right)^{-1} \times\sin\tau(\lambda_j - \lambda_i)(S^{T}T^{(s)}(\{u_k\},0)S)_{i,j} \times(S^{T}T^{(s)}(\{u_k\},0)S)_{j,i} \ , \tag{17}$$

where the matrix S diagonalizes the matrix $T^{(s)}(\{u_k\},\mu)$ and λ_i are the eigenvalues of $T^{(s)}(\{u_k\},\mu)$.
The second term in (15) can be worked out analytically and reads

$$2Z^{-1}{\sum_{i,j}}'\sum_{s}\int_{\{u_k\}}\rho(\{u_k\})\frac{\lambda_j - \lambda_i}{(\epsilon - i\omega)^2 + (\lambda_j - \lambda_i)^2} \times\left(1 + e^{\beta\lambda_i}\right)^{-1}(S^{T}T^{(s)}(\{u_k\},0)S)_{i,j} \times(S^{T}T^{(s)}(\{u_k\},0)S)_{j,i} \ , \tag{18}$$

where $\sum_{i,j}'$ denotes a summation over i and j such that $\lambda_i \neq \lambda_j$. The computation of $\sigma(\omega)$ takes of the order of L^2 operations. The statistical noise on $\sigma(\omega)$ is of the same order of magnitude as for the DOS and the static quantities.

In general, the real part of the conductivity may be written as $\sigma(\omega) = D\delta(\omega) + \sigma^{reg}(\omega)$ [19]. The coefficient D of the delta function is called the Drude weight and serves as a direct and sensitive measure of a metal-insulator transition [19–21]. If $D = 0$ the system is an insulator and otherwise it is a conductor. From (15) it immediately follows that the Drude weight cannot be larger than the absolute value of the hopping energy: $|D| \leq 2|\sum_{i\neq j}\sum_{s}\langle T^{(s)}(\{u_k\},\mu)_{i,j}c_{i,s}^{+}c_{j,s}\rangle|$. From (15) and (18) it can be seen that the Drude weight is given by

$$D = -2Z^{-1}\int_{\{u_k\}}\sum_{i\neq j}\sum_{s}\rho(\{u_k\},\mu)T^{(s)}(\{u_k\},0)_{i,j} \times\left(1 + e^{\beta T^{(s)}(\{u_k\},\mu)}\right)^{-1}_{i,j} +2Z^{-1}\int_{\{u_k\}}{\sum_{i,j}}'\sum_{s}\frac{1}{\lambda_j - \lambda_i}\left(1 + e^{\beta\lambda_i}\right)^{-1} \times(S^{T}T^{(s)}(\{u_k\},0)S)_{i,j}(S^{T}T^{(s)}(\{u_k\},0)S)_{j,i} \ . \tag{19}$$

4. The Su-Schrieffer-Heeger model

A detailed investigation of the properties of one-dimensional electron-phonon models is important to elucidate the connection between the models and various quasi-one-dimensional

real materials. One of the principal motivations for research on quasi-one-dimensional conductors has been the possibility of obtaining high-temperature superconductivity or at least very high conductivity from moving charge-density-waves (Fröhlich conductivity) [22].

We apply the method described above to calculate the single-particle and two-particle (optical, magnetic, superconducting) excitations for the Su-Schrieffer-Heeger (SSH) model, an electron-phonon model which is often used to describe the electronic properties of conjugated polymers [3–5]. The SSH model Hamiltonian reads [3–5, 23–26]

$$\begin{aligned}\mathscr{H} = &-\sum_i \sum_s \left(t - \alpha\left(u_{i+1} - u_i\right)\right)\left(c^+_{i,s}c_{i+1,s} + c^+_{i+1,s}c_{i,s}\right) \\ &-\mu \sum_i \sum_s n_{i,s} + \frac{1}{2M}\sum_i p_i^2 \\ &+\frac{K}{2}\sum_i \left(u_{i+1} - u_i\right)^2 \ , \end{aligned} \tag{20}$$

where $c^+_{i,s}$ and $c_{i,s}$ are the creation and annihilation operators, respectively, for a π-electron with spin $s =\uparrow,\downarrow$ at the i-th CH group, $n_{i,s}$ denotes the number operator at group i, μ is the chemical potential which fixes the number of π-electrons, u_i is the coordinate describing the displacement of the i-th CH group along the molecular symmetry axis, p_i is the corresponding momentum, t is the hopping integral for the undimerized chain, α is the electron-phonon coupling constant, K is the effective σ-spring constant and M is the total mass of the CH group [3–5, 23–26].
At half-filling one has for the ground-state energy [4,5]

$$\frac{\widetilde{E}_0}{L} = \min_z \left(-\frac{4t}{\pi}\mathscr{E}(1-z^2) + \frac{Kt^2z^2}{2\alpha^2}\right) \ , \tag{21}$$

where $\mathscr{E}(x)$ denotes the complete elliptic integral of the second kind and

$$\frac{E_0^{(p)}}{L} = \frac{1}{\pi}\sqrt{\frac{4K}{M}} \ . \tag{22}$$

For trans-polyacetylene we use a set of model parameters which is often adopted in model calculations [3–5]: t = 2.5 eV, α = 4.1 eV/Å, K = 21 eV/Å^2 and M = 3145 eV^{-1}/Å^2.

For this set of parameters one has [4,5] $\widetilde{E}_0/L$ = -3.170 eV and $E_0^{(p)}/L$ = 0.052 eV. From (10) it follows that

$$-3.170 \text{ eV} \le E_0/L \le -3.118 \text{ eV} \ , \tag{23}$$

giving support to the idea [3–5, 23–26] that a semi-classical treatment of the phonons may be a good starting point for the description of the electronic properties of polyacetylene.

5. Results

The results reported in this paper have been obtained from simulations of even-site rings containing up to 256 sites and 256 electrons, exceeding the length of most chains in actual materials [27–29]. Energies will be measured in units of t = 2.5 eV. Disregarding the statistical errors (which are too small to be visible on the figures presented below) the results for the static and dynamic properties (as obtained from a few statistically independent runs of 1000 samples each) are, for all practical purposes, numerically exact.

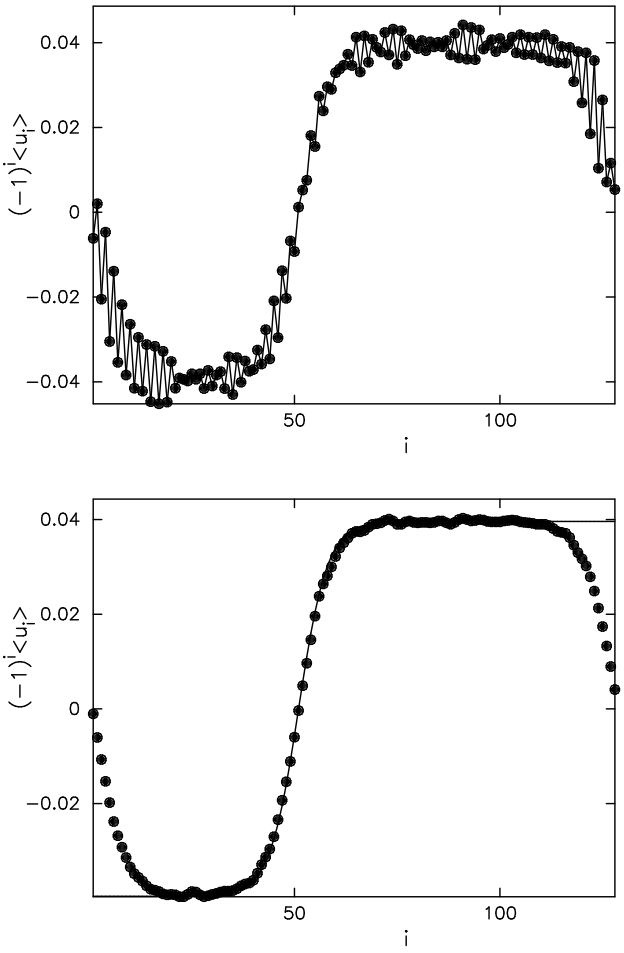

Fig. 1. a Lattice distortions for a ring of 128 sites for y = 0.016 and T = 2.9K. The line is a guide to the eye. **b** Same as **a**, but the smallest wave numbers are filtered out. Bullets: Simulation results; solid line: $u_0 \tanh\left[(i-i_0)/l\right]$

5.1. Low-temperature

First we demonstrate that our method reproduces the known features of the model at low-temperature (in practice we set T = 2.9K, corresponding to βt = 10000) [3–5, 23–26]. At half-filling the configuration $\{u_i\}$ with equal spacing between the CH groups is unstable with respect to a dimerization distortion, the Peierls instability [30], in which adjacent CH groups move toward each other forming alternately short and long bonds. Our numerical results for half-filled CH chains of 64, 128 and 256 sites show that the equilibrium bond alternation amplitude u_0 = 0.0409Å. This indicates that u_0 does not strongly depend on system size for the chain lengths considered in this work. In Fig. 1a we show the pattern of the lattice displacement for the case in which two electrons are taken away from a half-filled 128-site ring.

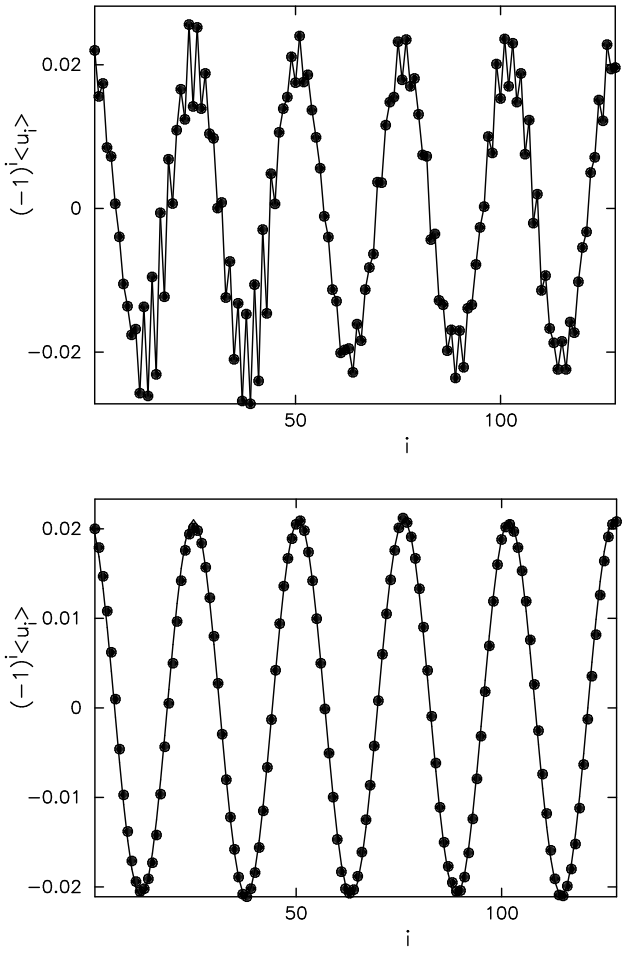

Fig. 2. **a** Lattice distortions for a ring of 128 sites for y = 0.078 and T = 2.9K. The line is a guide to the eye. **b** Same as **a**, but the smallest wave numbers are filtered out. Bullets: Simulation results; solid line: $u_0 \sin\left[2\pi m(i-i_0)/L\right]$

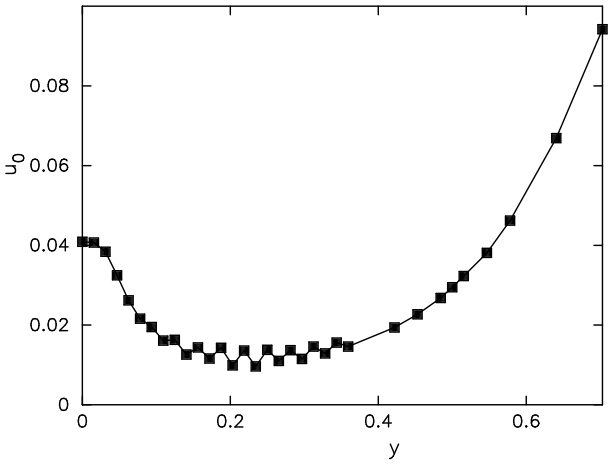

Fig. 3. Equilibrium bond alternation amplitude u_0 as a function of dopant concentration y for a ring of 128 sites and T = 2.9K. The line is a guide to the eye

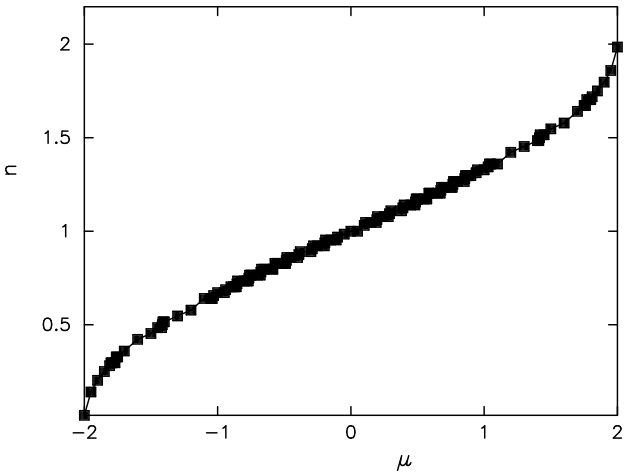

Fig. 4. Electron density n as a function of the chemical potential μ for a ring of 128 sites and T = 2.9K. The line is a guide to the eye

The dopant concentration $y \equiv 1-n$ = 0.016, where n is the density of electrons in the chain. The small oscillations on top of the superstructure can easily be removed by standard filtering procedures. The result is depicted in Fig. 1b. The solid curve in Fig. 1b is given by $u_i = u_0 \tanh[(i-i_0)/l]$ where i_0 is a fitting parameter, l = 8 determines the extent of the defect and u_0 = 0.0409Å. The hyperbolic tangent is characteristic of the bond-length alternation associated with the geometric distortion due to a soliton on an infinite chain [3–5, 23–26]. Variational calculations suggest a value of $l \approx 7$ [3–5, 24–26]. As expected, Fig. 1 shows that for the case in which two electrons are taken away from a half-filled 128-site ring, two solitons are being created. Simulations for the case in which four electrons are taken away from a half-filled 256-site chain (y = 0.016) show that four solitons are created and also give l = 8, indicating that the extent of the defect does not strongly depend on the size of the system. Upon doping the 128-site ring further the soliton lattice evolves toward a sinusoidal modulation as shown in Fig. 2 for y = 0.078. The solid curve in Fig. 2b is given by $u_i = u_0 \sin[2\pi m(i-i_0)/L]$, where i_0 and m are fitting parameters. Additional simulations for 64 and 256-site rings (results not shown) strongly suggest that solitons (soliton-antisoliton pairs) are only present for dopant concentrations $y < 0.031$ and that the transition from the soliton lattice to the sinusoidal modulation is continuous. This also implies (and is corroborated by our simulation data (not shown)) that systems of 64 sites or less cannot support soliton–antisoliton pairs because the removal of two electrons from the half-filled system corresponds to a dopant concentration that exceeds the critical value of 3.1%.

The equilibrium bond-length alternation amplitude u_0 as a function of the concentration y is shown in Fig. 3. For $y < 0.031$ the value of u_0 is the same as for the half-filled band. For $y > 0.031$, u_0 decreases from its half-filled band value and reaches a minimum value $u_0 \approx 0.01$Å for $y \approx 0.2$. Thereafter u_0 increases with increasing y and for $y > 0.58$, u_0 becomes even larger than its half-filled band value. Hence, this increase of u_0 is not due to y approaching 0.5, a concentration that corresponds to a modulation that is commensurate with the underlying lattice [31].

There is strong experimental evidence that upon doping trans-polyacetylene a first-order metal-insulator phase transition occurs at a dopant concentration of approximately 6% [29, 32]. A first-order phase transition is characterized by

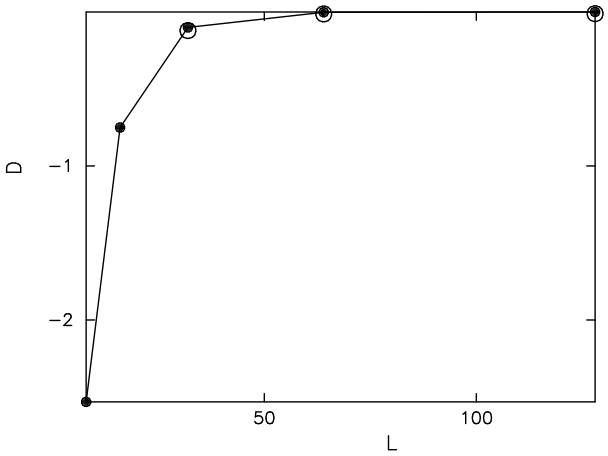

Fig. 5. Drude weight D as a function of the number of sites L. Bullets: D calculated from (27) with u_0 = 0.04Å, circles: Quantum molecular dynamics results for $T = 2.9K$, corresponding to $\beta t = 10000$. The line is a guide to the eye

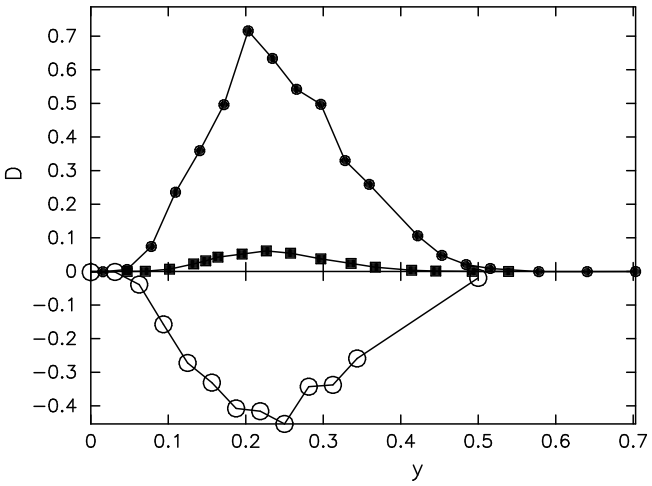

Fig. 6. Drude weight D as a function of the dopant concentration y for $T = 2.9K$. Bullets: L = 128, number of electrons $N = 4m + 2$; circles: L = 128, number of electrons $N = 4m$; squares: L = 256, number of electrons $N = 4m + 2$. The lines are guides to the eye

plateaus and steps in n versus μ [33]. Our numerical results, depicted in Fig. 4, show that n varies smoothly as a function of μ, strongly suggesting that the SSH model does not exhibit a first-order phase transition as a function of doping. The small steps in n versus μ indicate that at low-temperature only states with an even number of electrons are thermodynamically stable and that the formation of polarons is unlikely.

To explore the occurrence of a metal-insulator as a function of doping, we calculate the Drude weight and the optical conductivity. First we demonstrate that our method reproduces the optical conductivity and the insulating feature of the half-filled system at zero-temperature. The Hamiltonian which describes a completely dimerized chain is given by

$$H = t_+ \sum_{j,s} \left(c^+_{2j+1,s} c_{2j+2,s} + h.c. \right) + t_- \sum_{j,s} \left(c^+_{2j+2,s} c_{2j+3,s} + h.c. \right) \ , \qquad (24)$$

where $t_\pm = -t \pm 2\alpha u_0$. The optical conductivity for model (24) can be worked out analytically, yielding

$$\sigma(\omega) = \lim_{\epsilon \to 0} \frac{1}{\omega + i\epsilon} \times \left\{ - \sum_k \epsilon_k + 4 \sum_k \frac{\left(t_+^2 - t_-^2\right)^2}{\epsilon_k \left(\epsilon - i\omega\right)^2 + 4\epsilon_k^3} \right\} \ , \qquad (25)$$

where $\epsilon_k = -\sqrt{t_+^2 + t_-^2 + 2t_+ t_- \cos(4\pi k/L)}$. Extraction of the Drude weight gives for the dimerized chain

$$D = - \sum_k \epsilon_k + \left(t_+^2 - t_-^2\right)^2 \sum_k 1/\epsilon_k^3 \ . \qquad (26)$$

In Fig. 5 the Drude weight for the half-filled system is shown as a function of system size. Our quantum molecular dynamics results (circles) agree very well with the results obtained from (26) (bullets). The Drude weight for $L = 4m$-site rings is negative and goes to zero as the number of lattice sites increases. Systems with more than 64 sites are needed to obtain $D = 0$, as expected for a semiconductor at low-temperature. Our simulation technique also reproduces the exact values of $\sigma(\omega)$ as given by (25) (data not shown).

The behavior of the Drude weight D as a function of the dopant concentration y, is shown in Fig. 6 for rings of 128 sites. As seen above, at low temperature the system is unstable with respect to the removal (addition) of an odd number of electrons from (to) the half-filled system containing an even number of sites. Hence the number of electrons in the system N is given by $4m$ or $4m + 2$ where m is an integer number. At zero and low dopant concentration ($y < 0.06$) the Drude weight is zero. In the doping regime $0.06 < y < 0.5$ the Drude weight is strictly negative if the number of electrons is divisible by four and strictly positive otherwise. Physically a negative value for D corresponds to a negative inductance, or orbital paramagnetism [34]. Orbital paramagnetism also arises in a noninteracting dimerized model with $4m$-sites [35] and negative values for D have also been found in half-filled Hubbard rings with $4m$-sites [34, 36]. At very high dopant concentrations $y > 0.5$ the system becomes again insulating ($D = 0$). Comparing the results for $L = 128$ (bullets) and for $L = 256$ (squares), we expect for infinite chains the Drude weight to be zero for all dopant concentrations.

Figure 7 shows a series of calculated optical absorption spectra for various dopant concentrations. The optical absorption for the undoped case (thick solid line) has a gap. For dopant concentrations below 6%, a midgap absorption peak appears. The intensity of the midgap absorption peak comes from the interband transitions over the whole spectral range. For $y < 0.031$, i.e. the range of dopant concentrations for which the system supports solitons, the intensity of the midgap absorption is proportional to the dopant concentration. In the intermediate doping regime $0.031 < y < 0.06$ the doping dependence of the intensity of the midgap absorption changes. In the heavily doped regime ($y > 0.06$) the interband transition has completely disappeared. For all dopant concentrations the optical conductivity exhibits a gap at low frequencies. Hence for $0.06 < y < 0.5$ the system is not a simple metal. For $0.06 < y < 0.5$ the gap in $\sigma(\omega)$ first

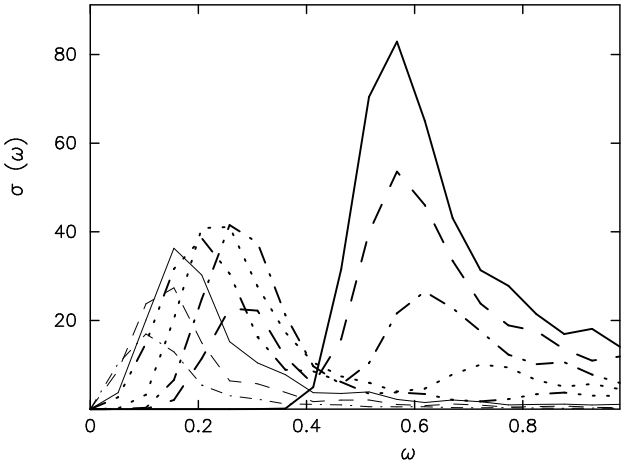

Fig. 7. Optical absorption $\sigma(\omega)$ for a ring of 128 sites for various dopant concentrations and T = 2.9K. Thick solid line: y = 0, thick dashed line: y = 0.016, thick dash-dotted line: y = 0.031, thick dotted line: y = 0.047, thick dash-triple dotted line: y = 0.063, thin solid line: y = 0.078, thin dashed line: y = 0.109, thin dash-dotted line: y = 0.328. ω is measured in units of t = 2.5 eV

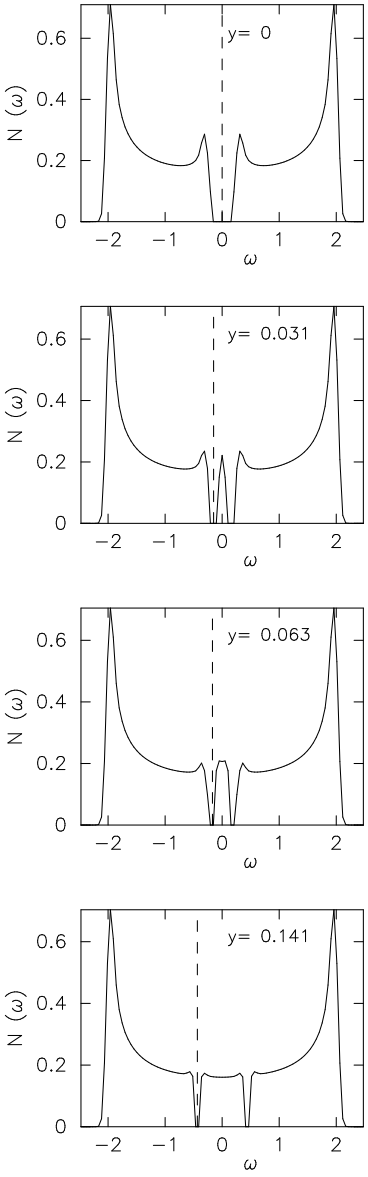

Fig. 8. Density of states $N(\omega)$ for a ring of 256 sites for various dopant concentrations y and T = 2.9K. The dashed line denotes the position of the chemical potential. ω is measured in units of t = 2.5 eV

decreases with doping, becomes minimal there where $|D|$ is maximal and then increases again.

To study the nature of the metal-insulator transition further, we also calculate the DOS. The DOS for the SSH model shows a gap Δ for all electron fillings and the chemical potential always falls in the gap [31, 37]. This is confirmed by the results shown in Fig. 8, where we show $N(\omega)$ for a ring of 256 sites for various dopant concentrations. At half-filling (y = 0), $N(\omega)$ consists of two bands separated by a gap Δ = 1.22 eV $\pm$ 0.02 eV [38]. The chemical potential is located in the middle of the gap and the system is a dimerized semiconductor. At low dopant concentration ($y < 0.06$) there is a narrow, mid-gap band in the DOS. For $y \leq 0.031$ this band is due to the presence of solitons whereas for $0.031 < y < 0.06$ it results from the sinusoidal modulation. At high dopant concentration ($y > 0.06$) the midgap-band broadens. There is excellent qualitative agreement between the results for the DOS obtained by a combination of geometry optimization and the continued fraction technique [31, 37] and our numerically exact results.

The DOS has a gap and the chemical potential is located within the gap even though the system is conducting for $0.06 < y < 0.5$. Therefore the system is not a conventional conductor. In Fig. 9 we show the gap Δ in $N(\omega)$ as a function of dopant concentration for electron fillings $N = 4m+2$. The gap Δ in $N(\omega)$ equals the gap in $\sigma(\omega)$. Our results (not shown) for the Pauli susceptibility χ_P (for $L = 128, 256$ and for all dopant concentrations) clearly demonstrate that χ_P = 0, as might be expected on the basis of the free-electron theory in which χ_P is proportional to the DOS at the chemical potential [39]. Note however that in the SSH model the electrons interact.

The observation that the DOS has a gap and the chemical potential is located within the gap even though the system is conducting for $0.06 < y < 0.5$ does not have to be inconsistent. Indeed, a BCS superconductor [39] and a Fröhlich conductor [40] exhibit the same characteristics. Superconductivity is characterized by the existence of off-diagonal long-range order (ODLRO) [41]. Fröhlich conductivity requires a periodic lattice distortion incommensurate with the lattice and an accompanying periodic distortion in the conduction electron charge density: a charge-density-wave (CDW) [40]. Although a purely one-dimensional system with short-range interactions cannot undergo a phase transition at any finite temperature [42], it may exhibit long-range order at T = 0. However, the question of order in a chain can be discussed in terms of its tendency towards long-range order as $T \to 0$ because even though there is no long-range order at $T \neq 0$, it is possible for very-long-range (but finite) correlations to build up.

We first examine the possibility of having Fröhlich conductivity in the SSH model. At half-filling the configuration with equal spacing between the sites is unstable with respect to a Peierls instability [30]. A dimerization distortion with wavevector $q = 2q_F$ with $q_F = (\pi/2)(1 \pm y)$ results. In the

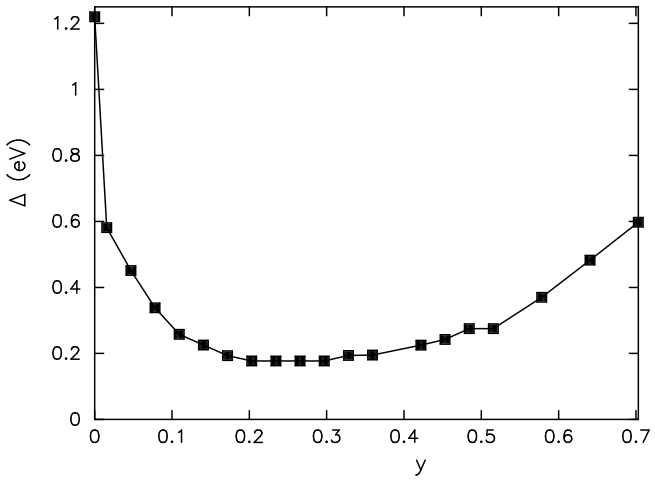

Fig. 9. Gap Δ in the density of states $N(\omega)$ as a function of the dopant concentration y for a ring with 128 sites and $T = 2.9K$. The line is a guide to the eye

doping regime $0 \leq y < 0.5$ we also observe a CDW with wave vector $q = 2q_F$. For $y > 0.5$ a $2q_F$ CDW with higher harmonics appears. Thus for $0.06 < y < 0.5$ the finite Drude weight may be explained by the Fröhlich conducting mechanism: The lattice and electronic charge distortion move as one travelling wave.

Criteria which may be used to decide whether or not a given model exhibits superconductivity is the occurrence of flux quantization [41, 43] or a non-zero value of the superfluid density ρ_s [21]. To explore flux quantization we thread a magnetic flux ϕ through the center of the ring. As a consequence the hopping term in (20) acquires a constant phase $\exp(\pm 2\pi i\phi/L\phi_0)$ where $\phi_0 = hc/e$ is the flux quantum [44]. Byers and Yang argue that, in the thermodynamic limit, the functional form of the grand potential $\Omega = -\beta^{-1} \ln Z$ as a function of ϕ allows one to distinguish between a normal metal and a superconductor [41, 43]. In the case of a superconductor $\Omega(\phi)$ is an even periodic function of ϕ with period ϕ_0/k where k stands for the sum of charges of the particles in the basic group [41]. The resulting flux dependence requires that a superconductor exhibits ODLRO [41]. On the other hand, the curve $\Omega(\phi)$ is flat in the case of a normal metal. The superfluid density ρ_s can be calculated from the dependence of the grand potential on ϕ using $\rho_s \propto L^{-1}(\partial^2\Omega(\phi/L)/\partial(\phi/L)^2)_{\phi/L=0}$ [21, 45–48]. A feeling for the system-size dependence of ρ_s can be obtained by considering a free electron system. Evidently in that case one expects to find $\rho_s = 0$, independent of the dimension and the temperature. For a one-dimensional free electron system

$$\left.\frac{\partial^2\Omega}{\partial(\phi/L)^2}\right|_{\phi/L=0} = 2t\sum_k n_k \cos k - 2\beta t\sum_k n_k(1-n_k)\sin^2 k \ , \qquad (27)$$

with

$$n_k = \frac{1}{e^{\beta(-2t\cos k-\mu)}+1} \ . \qquad (28)$$

Numerical results for the r.h.s. of (27) for various system sizes and inverse temperatures for $t = 1$ and $n = 1$ are given

Table 1. Superfluid density ρ_s for the half-filled one-dimensional free electron system as a function of system size L and inverse temperature β

L	$\beta = 10$	$\beta = 100$	$\beta = 1000$
16	−0.626	−11.872	−124.37
18	0.386	0.640	0.639
32	−0.087	−5.615	−61.865
34	0.066	0.638	0.638
36	−0.052	−4.921	−54.921
64	−0.001	−2.489	−30.614
66	0.001	0.635	0.637
72	0.000	−2.141	−27.142
1024	0.000	0.000	−1.312
1026	0.000	0.000	0.603
10000	0.000	0.000	0.000

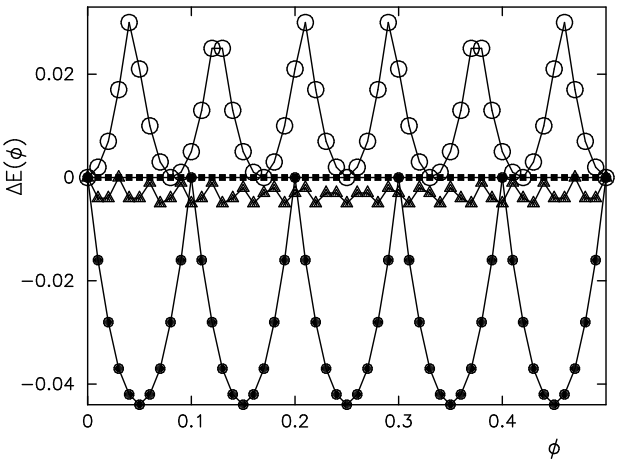

Fig. 10. $\Delta E(\phi)$ for free fermions at zero temperature. Bullets: 12-site ring, circles: 14-site ring; triangles: 36-site ring; squares: 128-site ring. The lines are guides to the eye

in Table 1. For all temperatures $\rho_s \leq 0$ for $L = 4m$ and $\rho_s \geq 0$ for $L = 4m + 2$ where m is an integer number. This change of sign of ρ_s with L is similar to the behavior found in the Drude weight [34, 36]. At very low temperatures very large system sizes are needed to obtain $\rho_s = 0$, as expected for the free electron system [49]. The system size required to yield a vanishing ρ_s grows with the inverse temperature, a feature which makes it difficult to decide whether or not the system is a superconductor. Therefore we decided to use flux quantization to rule out superconductivity in this system.

First we demonstrate that our method reproduces the flat $\Omega(\phi)$ curve for the free fermion system at zero-temperature (i.e. $\Omega(\phi) = E(\phi)$, $E(\phi)$ being the ground-state energy). In Fig. 10 we plot the energy difference $\Delta E(\phi) \equiv E(\phi) - E(\phi = 0)$ for free fermions on a ring of 12 (bullets), 14 (circles), 36 (triangles) and 128 (squares) sites. For small systems $\Delta E(\phi)$ clearly exhibits periodic behavior as a function of ϕ. This implies the presence of persistent currents ($J \propto \partial E/\partial\phi$), a well-known phenomenon in mesoscopic normal-metal rings [50–53]. Also clear from Fig. 10 is that the signal for flux quantization strongly depends on system-size: For a ring of 128 sites $\Delta E(\phi)$ is flat (up to four digits at least). Therefore the question of flux quantization can only be addressed by calculating $\Delta E(\phi)$ for sufficiently large systems. Our results for the SSH model for $L = 128, 256$ and for all dopant concentrations lie on top of the squares in Fig. 10, demonstrating that $\Delta E(\phi)$ is perfectly flat. Hence

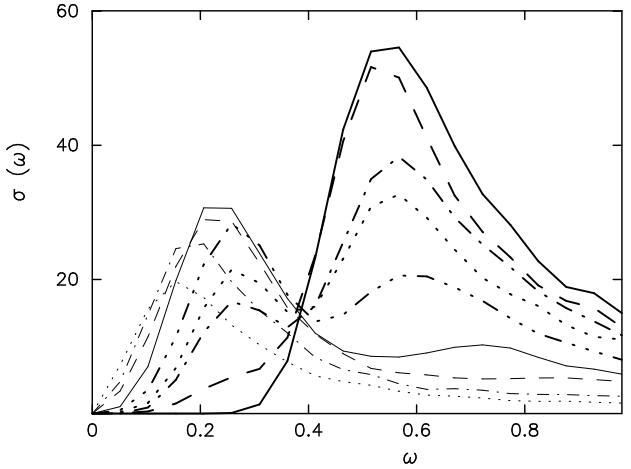

Fig. 11. Optical absorption $\sigma(\omega)$ for a ring of 128 sites for various dopant concentrations and T = 290K. Thick solid line: y = 0, thick dashed line: y = 0.008, thick dash-dotted line: y = 0.016, thick dotted line: y = 0.02, thick dash-triple dotted line: y = 0.031, thin solid line: y = 0.047, thin dashed line: y = 0.063, thin dash-dotted line: y = 0.078, thin dotted line: y = 0.109. ω is measured in units of t = 2.5 eV

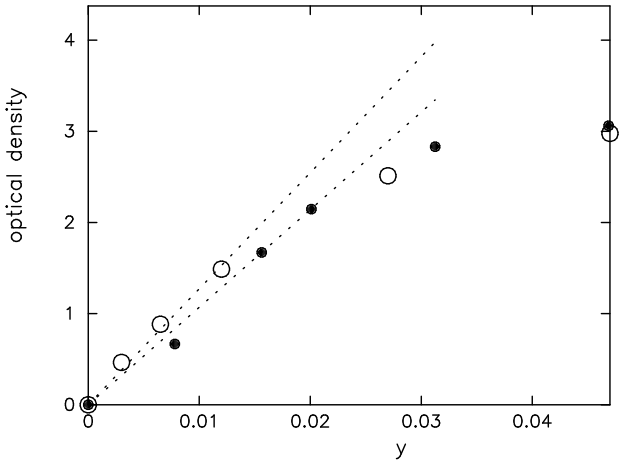

Fig. 12. Concentration dependence of the midgap optical absorption (arbitrary units). Circles: Experimental data [55]. Bullets: Simulation data taken from Fig. 11. The dotted lines are a guide to the eye

there is no flux quantization in the SSH model. This implies that ρ_s = 0 for all electron fillings. Hence the SSH model for 0.06 $< y <$ 0.5 provides an example for which the DOS and the optical absorption spectrum have a gap and $D \neq L\rho_s$ [21].

5.2. Room-temperature

To make contact with experimental work on trans-polyacetylene we calculate the optical conductivity for the SSH model at room-temperature. The optical absorption spectra $\sigma(\omega)$ at room-temperature (in practice we set T = 290K, corresponding to βt = 100) for various dopant concentrations y are depicted in Fig. 11 for rings of 128 sites. For the undoped case (thick solid line) $\sigma(\omega)$ shows an interband transition peak at ω = 1.42 eV $\pm$ 0.13 eV. Upon doping and for dopant concentrations below 6%, a midgap absorption peak appears at ω = 0.64 eV $\pm$ 0.13 eV. The intensity of

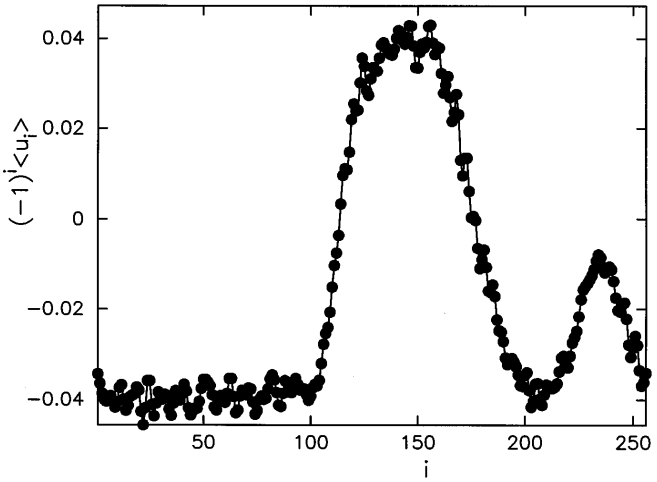

Fig. 13. Lattice distortion for a ring of 256 sites for y = 0.012 (3 electrons removed from the half-filled ring) and T = 290K. The line is a guide to the eye

the midgap absorption peak comes from the interband transition over the whole spectral range. The optical conductivities for different dopant concentrations ($y < 0.06$) cross in one point (the isosbestic point) at ω = 1.03 eV $\pm$ 0.13 eV. These features are also observed experimentally [54–56]. However, the calculated peak positions and isosbestic point are at slightly lower energies than found in experiment. In Fig. 12 we show the intensity of the midgap absorption peak (optical density) as a function of dopant concentration for $y < 0.06$. Our numerical results (bullets) indicate that for $y < 0.031$ the intensity of the midgap absorption peak increases linearly with the dopant concentration. In the intermediate doping regime $0.031 < y < 0.06$, the doping dependence of the intensity of the midgap absorption changes. Similar behavior is seen in the optical absorption measurements of Feldblum *et al.* [55] (circles). However, our results show that for $0.031 < y < 0.06$ the midgap absorption peak becomes higher than the interband transition peak, in disagreement with some experiments [54–56] but in agreement with others [57]. In the heavily doped regime ($y > 0.06$) the low-energy absorption shrinks with increasing dopant concentration and the corresponding peak shifts toward lower energy, while the interband transition completely disappears (see Fig. 11).

At low temperature a system containing an even number of sites has only states with an even number of electrons. Moderate doping ($y < 0.031$) results in the creation of soliton-antisoliton pairs only [11]. At room temperature this is no longer the case: The system is thermodynamically stable with respect to the removal of a single (or odd number of) electron(s), independent of the filling. Our calculations show that for moderate doping and an odd number of electrons, the thermodynamically relevant states consist of configurations with a single polaron and/or soliton-antisoliton pairs, an example being shown in Fig. 13. From Fig. 11 it is clear that the optical conductivity for systems containing a polaron (see the thick dashed and thick dotted line) does not show any extra features compared to the conductivity of systems without a polaron. Further evidence for this is provided by the data shown in Fig. 12 (second and fourth

bullet, counting from left to right). Our results for the density of states (not shown) indicate that both the polaron and the soliton-antisoliton pairs contribute to the weight at $\omega = 0$ [4].

6. Summary

A simulation method has been presented to compute the static and dynamic properties of electron-phonon models. The technique has been applied to the Su-Schrieffer-Heeger model at low and room-temperature. We have demonstrated that at low-temperature the Su-Schrieffer-Heeger model exhibits a metal-insulator transition as a function of the doping. The metallic state exhibits features characteristic of Fröhlich conductivity. Our simulation data for the optical absorption at room-temperature are in good agreement with experiment.

This work is supported by EEC contracts and a supercomputer grant of the "Stichting Nationale Computer Faciliteiten (NCF)".

References

1. A. Alavi, and D. Frenkel, J. Chem. Phys. **97**, 9249 (1992)
2. A. Yoshida, T. Døssing, and M. Manninen, J. Chem. Phys. **101**, 3041 (1994)
3. Conjugated Conducting Polymers, ed. H. Kiess. Berlin: Springer 1992
4. A.J. Heeger, S. Kivelson, J.R. Schrieffer, and W.-P. Su, Rev. Mod. Phys. **60**, 781 (1988)
5. Yu Lu, Solitons & Polarons in Conducting Polymers. Singapore: World Scientific 1988
6. L.M. Falicov and J.C. Kimball, Phys. Rev. Lett. **22**, 997 (1969)
7. T. Kennedy and E.H. Lieb, Physica **A138**, 320 (1986)
8. J. Jedrzejewski, J. Lach, and R. Lyzwa, Physica **A154**, 529 (1989)
9. R. Car and M. Parinello, Phys. Rev. Lett. **55**, 2471 (1985)
10. A. Alavi, J. Kohanoff, M. Parinello, and D. Frenkel, Phys. Rev. Lett. **73**, 2599 (1994)
11. H. De Raedt, Proceedings of the Como Summer School on Monte Carlo and Molecular Dynamics of Condensed Matter Systems. edited by K. Binder and G. Ciccotti, (Società Italiana di Fisica, Bologna, 1996)
12. S. Golden, Phys. Rev. **137**, 1127 (1965)
13. K. Symanzik, J. Math. Phys. **6**, 1155 (1965)
14. C.J. Thompson, J. Math. Phys. **6**, 1812 (1965)
15. E.F. Beckenbach, and R. Bellman, Inequalities. (Springer, Berlin, 1961)
16. L. Landau and E. Lifshitz, Physique Statistique. (Edition Mir 1967)
17. W. von der Linden, Phys. Rep. **220**, 53 (1992)
18. R. Kubo, J. Phys. Soc. Jpn. **12**, 570 (1957)
19. W. Kohn, Phys. Rev. **133**, A171 (1964)
20. B.S. Shastry and B. Sutherland, Phys. Rev. Lett **65**, 243 (1990)
21. D.J. Scalapino, S.R. White, and S. Zhang, Phys. Rev. B **47**, 7995 (1993)
22. J. Bardeen, Highly Conducting One-Dimensional Solids. edited by J.T. Devreese, R.P. Evrard, and V.E. Van Doren. New York: Plenum Press 1979
23. M.J. Rice, Phys. Lett. **71A**, 152 (1979)
24. W.P. Su, J.R. Schrieffer, and A.J. Heeger, Phys. Rev. Lett. **42**, 1698 (1979)
25. W.P. Su, J.R. Schrieffer, and A.J. Heeger, Phys. Rev. **B22**, 2209 (1980)
26. W.P. Su, J.R. Schrieffer, and A.J. Heeger, Phys. Rev. **B28**, 1138 (1983)
27. J.E. Hirsch and M. Grabowski, Phys. Rev. Lett. **52**, 1713 (1984)
28. H. Thomann, L.R. Dalton, Y. Tomkiewicz, N.S. Shiren and T.C. Clarke, Phys. Rev. Lett. **50**, 533 (1983)
29. M. Winokur, Y.B. Moon, A.J. Heeger, J. Barker, D.C. Bott, and H. Shirakawa, Phys. Rev. Lett. **58**, 2329 (1987)
30. R.E. Peierls, Quantum Theory of Solids. Oxford: Clarendon Press 1955
31. E.J. Mele and M.J. Rice, Phys. Rev. B **23**, 5397 (1981)
32. J. Chen, T.-C. Chung, F. Moraes, and A.J. Heeger, Solid State Comm. **53**, 757 (1985)
33. L.E. Reichl, A Modern Course in Statistical Physics. (Edward Arnold, London, 1980)
34. C.A. Stafford, A.J. Millis, and B.S. Shastry, Phys. Rev. B **43**, 13660 (1991)
35. J.A. Pople and K.G. Untch, J. Am. Chem. Soc. **88**, 4811 (1966)
36. R.M. Fye, M.J. Martins, D.J. Scalapino, J. Wagner, and W. Hanke, Phys. Rev. B. **44**, 6909 (1991)
37. M.J. Rice and E.J. Mele, Chem. Scr. **17**, 121 (1981)
38. The resolution used to draw the DOS is too low to permit an accurate determination of the gap. The value quoted has been obtained from the original data
39. G.D. Mahan, Many-Particle Physics. New York: Plenum Press 1981
40. H. Fröhlich, Proc. Roy. Soc. **A223**, 296 (1954)
41. C.N. Yang, Rev. Mod. Phys. **34**, 694 (1962)
42. L. Van Hove, Physica **16**, 137 (1950)
43. N. Byers and C.N. Yang, Phys. Rev. Lett. **7**, 46 (1961)
44. F. London, J. Phys. Rad. **8**, 397 (1937)
45. M.E. Fisher, M.N. Barber, and D. Jasnow, Phys. Rev. A **8**, 1111 (1973)
46. P.J.H. Denteneer, Guozhong An, and J.M.J. van Leeuwen, Phys. Rev. B **47**, 6256 (1993)
47. F.F. Assaad, W. Hanke, and D.J. Scalapino, Phys. Rev. B **50**, 12835 (1994)
48. J.M.J. van Leeuwen, M.S.L. du Croo de Jongh, and P.J.H. Denteneer, J. Phys. A: Math. Gen. **29**, 41 (1996)
49. Although we presented some results for a one-dimensional system only, the same conclusion holds for a two- or three-dimensional system
50. M. Büttiker, Y. Imry, and R. Landauer, Phys. Lett. **96A**, 365 (1983)
51. H.F. Cheung, E. Riedel, and Y. Gefen, Phys. Rev. Lett. **62**, 587 (1989)
52. H. Bouchiat and G. Montambaux, J. Phys. (Paris) **50**, 2695 (1989)
53. L.P. Lévy, G. Dolan, J.Dunsmir, and H. Bouchiat, Phys. Rev. Lett. **64**, 2074 (1990)
54. N. Suzuki, M. Ozaki, S. Etemad, A.J. Heeger, and A.G. Mac-Diarmid, Phys. Rev. Lett. **45**, 1209 (1980)
55. A. Feldblum, J.H. Kaufman, S. Etemad, and A.J. Heeger, Phys. Rev. B **26**, 815 (1982)
56. T.-C. Chung, F. Moreas, J.D. Flood, and A.J. Heeger, Phys. Rev. B **29**, 2341 (1984)
57. S. Hasegawa, M. Oku, M. Shimizu, and J. Tanaka, Synth. Met. **38**, 37 (1994)